AIMS Mathematics

https://www.aimspress.com/journal/Math

AIMS Mathematics, 11(8): 26590–26612.
DOI:10.3934/math.20261066
Received: 21 May 2026
Revised: 03 August 2026
Accepted: 05 August 2026
Published: 25 August 2026

Research article

Predefined-time fractional-order sliding-mode control for UAV attitude tracking under disturbances

Saim Ahmed[1,3,*], **Ahmad Taher Azar**[1,2] **and Rozaimi Ghazali**[3,*]

[1] Automated Systems and Computing Lab (ASCL), Prince Sultan University, Riyadh, Saudi Arabia

[2] College of Computer and Information Sciences, Prince Sultan University, Riyadh, Saudi Arabia

[3] Centre for Robotics and Industrial Automation (CeRIA), Fakulti Teknologi dan Kejuruteraan Elektrik (FTKE), Universiti Teknikal Malaysia Melaka, Hang Tuah Jaya 76100, Durian Tunggal, Melaka, Malaysia

* **Correspondence:** Email: sahmed@psu.edu.sa, rozaimi.ghazali@utem.edu.my.

Abstract: Unmanned aerial vehicles (UAVs) are important for various civil and industrial tasks, including package delivery, crop inspection, and disaster assessment. These applications require precise course tracking and reliable performance under adverse weather conditions, including high winds, payload variations, and modeling uncertainties. Classical robust control methods, such as sliding mode control (SMC), are widely favored for their robustness against uncertain dynamics. However, conventional SMC suffers from chattering and may exhibit relatively slow convergence. Finite-time sliding-mode control (FTSMC) algorithms improve the convergence rate; however, their settling time depends on the initial conditions. Predefined-time fractional-order sliding mode control (PFSMC) ensures state convergence within a designer-specified interval. In this paper, a comprehensive study of the PFSMC for UAV systems is presented. A dynamic model of the UAVs is presented, a control rule with predefined time guarantees is proposed, and a Lyapunov theory is used to guarantee stability. The proposed PFSMC is simulated and compared with FTSMC, fixed-time SMC (FxSMC), and fractional FxSMC (FFxSMC), demonstrating improved robustness, tracking performance, and reduced chattering. The results show that the PFSMC is an optimal control method for UAV systems when robustness and predefined-time guarantees are required.

Keywords: UAV; fractional-order control; predefined-time; sliding mode control; attitude control
Mathematics Subject Classification: 93B52, 93C10, 93C40, 93D09, 93D21

1. Introduction

Over the last ten years, unmanned aerial vehicles (UAVs) have evolved from experimental prototypes to important tools for both civilian and military applications [1]. They are suitable for a wide range of applications, including infrastructure inspection, environmental monitoring, package transportation, border surveillance, and aerial cinematography, owing to their flexibility, vertical takeoff capability, and relatively low deployment cost. As this becomes increasingly important, there is a considerable need for control methods that ensure accuracy and robustness, especially in challenging environmental conditions [2].

A main control problem arises from the strongly coupled nonlinear and underactuated dynamics of the quadrotor UAV design [3]. This complexity is further compounded by operational issues such as wind turbulence, varying payload distributions, actuator delays, and external noise. Standard linear controllers such as PID, H_∞, and LQR are simple to implement, but often their performance suffers if the system deviates from the nominal equilibrium condition [4,5]. This has led to an increasing interest in robust nonlinear control approaches.

Sliding mode control (SMC) has been widely recognized for its robustness against matched disturbances and modeling uncertainties [6]. The fundamental principle of SMC is to drive the system states to a carefully designed sliding surface and maintain them there using a discontinuous control law. Once the system reaches the sliding surface, the resulting sliding dynamics become insensitive to matched uncertainties and disturbances. However, conventional SMC generally cannot fully compensate for unmatched uncertainties, thereby still affecting system performance. Despite these advantages, SMC has several limitations. The most prominent is the well-known phenomenon of chattering, in which high-frequency oscillations in the control signal can cause mechanical wear, excite unmodeled dynamics, or degrade actuator performance. To mitigate this issue, numerous techniques, including higher-order sliding mode control and boundary-layer approaches, have been proposed, each providing a different tradeoff between robustness and control smoothness.

Fractional calculus is an extension of the classical calculus where differentiation and integration are generalized to arbitrary (noninteger) orders [7, 8]. It has become a powerful mathematical tool in control system design due to its capacity to improve robustness, transient response, and tracking performance [9]. Fractional-order sliding mode control is an extension of the classical sliding mode control that uses fractional-order derivatives and integrals, which provide more design flexibility [10]. The fractional operators have nonlocal memory properties in contrast to the integer-order operators, which helps to understand the inherited and frequency-dependent behavior of UAVs under the effect of aerodynamic disturbance more efficiently [11, 12]. Thus, the addition of fractional-order sliding surfaces to the sliding mode control scheme improves robustness, reduces chattering, and enhances the accuracy of the trajectory tracking.

Motivated by the theory of finite-time stability, finite-time sliding mode control (FTSMC) was developed to ensure that system trajectories converge to the equilibrium within a finite time rather than asymptotically [13]. Compared with conventional sliding mode control, FTSMC improves convergence speed and robustness against disturbances. However, its settling time remains dependent on the initial conditions, making it difficult to establish a priori convergence bounds. To overcome this limitation, fixed-time and faster fixed-time control strategies have been developed to guarantee convergence within a prescribed upper bound that is independent of the initial states. These approaches have been successfully applied to a wide range of nonlinear mechanical systems, including Euler–Lagrange systems, robotic manipulators, and autonomous surface vessels [14–16].

More recently, prescribed-time and predefined-time control strategies have emerged as promising approaches for mission-critical operations requiring explicit, user-defined temporal boundaries, such as close-proximity drone swarms or automated collision avoidance [17, 18]. By decoupling the maximum settling time parameter from both the initial system states and internal control gains, predefined-time sliding mode techniques ensure deterministic convergence within a predefined time [19]. Although predefined-time fractional-order sliding mode control has demonstrated promising theoretical performance in recent years [20], its application to quadrotor UAV attitude control remains limited. Existing studies primarily consider generic nonlinear systems or robotic manipulators and seldom address the coupled nonlinear dynamics, aerodynamic disturbances, and robust transient-performance requirements inherent to UAV platforms. Moreover, few investigations provide an integrated framework encompassing controller synthesis, Lyapunov-based stability analysis, and systematic comparisons with established finite-time and fixed-time sliding mode controllers. Therefore, the development of an efficient PFSMC strategy that guarantees deterministic tracking performance for nonlinear quadrotor UAVs remains an open research challenge.

To better illustrate the motivation for the proposed controller, the main characteristics of representative sliding mode control strategies are summarized below:

- **Classical SMC:** Employs integer-order sliding surfaces and provides robust performance against matched uncertainties. However, it does not exploit fractional-order memory characteristics and often suffers from severe chattering due to high-gain discontinuous switching. Depending on the sliding manifold design, the tracking error exhibits asymptotic convergence ($t \to \infty$).
- **Finite-time SMC (FTSMC):** Guarantees state stabilization within a finite time, thereby improving transient performance over asymptotic approaches. Nevertheless, the calculated settling time depends explicitly on the initial conditions $x(0)$, and the discontinuous control action can still induce undesirable chattering.
- **Fixed-time SMC (FxSMC):** Ensures tracking convergence within a uniformly bounded time independent of the initial conditions, where the upper limit is determined strictly by the controller parameters. However, it relies on standard integer-order derivatives and lacks memory features to capture past system history.
- **Proposed PFSMC:** Achieves predefined-time convergence by ensuring that the tracking error fully settles within a user-specified time parameter T_p, completely independent of $x(0)$. Furthermore, by incorporating fractional-order operators, the controller exploits nonlocal memory effects to improve transient accuracy. Crucially, the low-pass smoothing properties inherent to the fractional integration phase significantly attenuate high-frequency chattering without sacrificing robust disturbance rejection.

The main contributions of this work are summarized as follows:

1) A predefined-time fractional-order sliding mode controller is developed for nonlinear quadrotor attitude dynamics. The proposed controller explicitly accounts for the coupled nonlinear attitude dynamics and bounded aerodynamic disturbances encountered in UAV applications, demonstrating the applicability of predefined-time fractional-order control to nonlinear quadrotor UAV attitude dynamics.

2) A sliding manifold guaranteeing predefined-time convergence is constructed by incorporating fractional-order operators. The proposed design exploits the nonlocal memory properties of fractional calculus to improve transient-tracking accuracy while mitigating chattering without compromising robustness.
3) Sufficient stability conditions are derived using Lyapunov theory to prove that all closed-loop tracking errors converge within a predefined time independent of the initial conditions.
4) Extensive numerical studies under reference-tracking and disturbance scenarios demonstrate that the proposed PFSMC consistently outperforms finite-time SMC, fixed-time SMC, and fractional-order fixed-time SMC in terms of tracking accuracy, control smoothness, disturbance rejection, and convergence within the predefined time.

The rest of the paper is organized as follows: Preliminaries are given in Section 2. Section 3 examines the model and its operation. Section 4 describes the proposed PFSMC design. Section 5 investigates closed-loop stability research employing Lyapunov theory. Section 6 presents simulations that support our method. The conclusion is given in Section 7.

2. Preliminaries

Lemma 1. [21] It is found that the Lyapunov function $\mathcal{L}(x)$ is predefined-time stable for the initial condition $\mathcal{L}_0$ if

$$\dot{\mathcal{L}}(x) \leq -c_1\mathcal{L}(x)^{1+\frac{\eta}{2}} - c_2\mathcal{L}(x)^{1-\frac{\eta}{2}}$$

where $c_1, c_2 > 0$, and $0 < \eta < 1$. The predefined settling time is given by

$$T_p = \frac{\pi}{\eta\sqrt{c_1 c_2}} \tag{2.1}$$

Remark 1. The predefined-time stability criterion established in Lemma 1 offers a significant advantage over conventional finite-time and fixed-time stability frameworks. In finite-time control, the settling time depends explicitly on the initial conditions and generally increases with larger initial state deviations. Fixed-time control overcomes this limitation by guaranteeing convergence within a uniform upper bound independent of the initial conditions. However, this upper bound is typically determined by multiple coupled controller parameters, making it less intuitive to satisfy specified mission-time requirements through controller tuning. In contrast, Lemma 1 provides an exact, explicit relationship that directly assigns and computes the predefined convergence time T_p. Consequently, the system states are guaranteed to converge to the equilibrium within the predefined time T_p, establishing a direct link between controller design and mission-specific timing requirements for UAV applications.

Lemma 2. [22] The inequalities for v_i can be given as follows:

$$\begin{aligned} &\sum_{i=1}^{n}|v_i|^{1+\eta} \geq \left(\sum_{i=1}^{n}|v_i|^2\right)^{\frac{1+\eta}{2}}, \ if\ 0 < \eta < 1 \\ &\sum_{i=1}^{n}|v_i|^{\eta} \geq n^{1-\eta}\left(\sum_{i=1}^{n}|v_i|\right)^{\eta}, \ if\ \eta > 1. \end{aligned} \tag{2.2}$$

Definition 1. [23] Fractional calculus is frequently used employing the Riemann–Liouville (RL) formulation. The fractional integral and derivative are thus defined as

$$
\begin{aligned}
{}_a\mathcal{I}_t^{\sigma} f(t) &= \frac{1}{\Gamma(\sigma)} \int_a^t \frac{f(\rho)}{(t-\rho)^{1-\sigma}} d\rho \\
{}_a\mathcal{D}_t^{\sigma} f(t) &= \frac{d^{\sigma} f(t)}{dt^{\sigma}} = \frac{1}{\Gamma(1-\sigma)} \frac{d}{dt} \int_a^t \frac{f(\rho)}{(t-\rho)^{\sigma}} d\rho
\end{aligned} \tag{2.3}
$$

with $m-1<\sigma<m$, $m \in \mathfrak{R}$. $\Gamma(\cdot)$ is the Euler gamma function, and it is given by

$$
\Gamma(\sigma) = \int_0^{\infty} e^{-t} t^{\sigma-1} dt
$$

whereas $\mathcal{I}$ is the fractional-order integral, and $\mathcal{D}$ is the fractional-order derivative.

Property 1. [12] The Riemann–Liouville derivative corresponds to the subsequent equality:

$$
\mathcal{D}^{\sigma}(\mathcal{D}^{-\sigma} f(t)) = f(t) \tag{2.4}
$$

3. System dynamics

The quadrotor UAV is modeled as a rigid body, exhibiting rotational motion defined by three degrees of freedom: roll, pitch, and yaw angles [24]. The dynamics of attitude control are inherently nonlinear and significantly interconnected under uncertainty. A detailed mathematical model of attitude dynamics is essential for developing robust attitude control methods. Figure 1 illustrates the relationship between the body coordinate system and the inertial coordinate system.

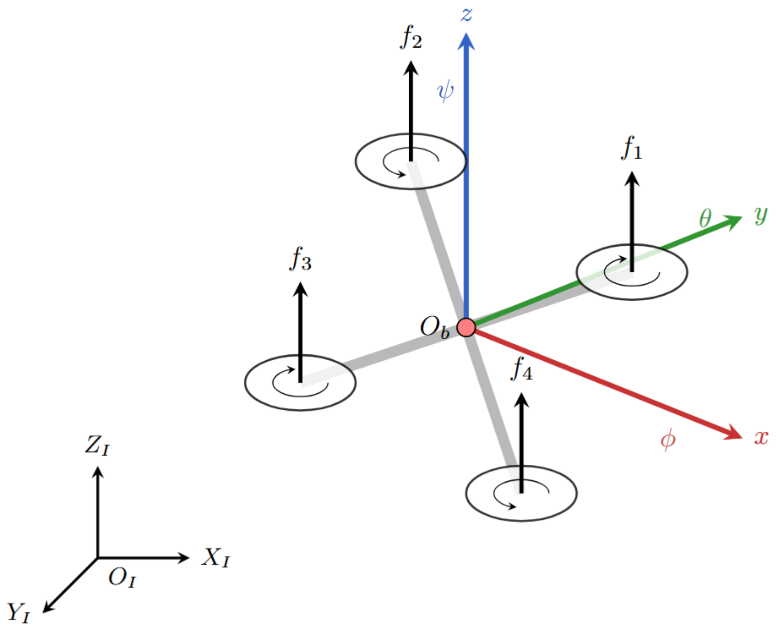

Figure 1. Quadrotor inertial and body coordinate diagram.

3.1. UAV attitude dynamics

Assumption 1. The quadrotor is considered a perfectly symmetric rigid body, with its center of mass precisely aligned with its geometric center of gravity.

Assumption 2. The variation in propeller dynamics during rotation is ignored, and the motor's reverse torque is not considered.

The torque balance equation that controls the quadrotor UAV's attitude motion, according to rigid body dynamics, is written as

$$\mathbf{M} = I\dot{\omega} + \omega \times (I\omega) \tag{3.1}$$

Here, I represents the moment of inertia matrix of the quadrotor, and $\omega = [p, q, r]^T$ designates the angular velocity vector, where p, q, and r correspond to the angular velocities around the body-fixed axes X_b, Y_b, and Z_b, respectively. The symbol $\mathbf{M}$ represents the resultant control moment exerted on the quadrotor.

We can write the control moment parts along the three body-fixed axes as follows:

$$\begin{bmatrix} M_x \\ M_y \\ M_z \end{bmatrix} = \begin{bmatrix} I_x\dot{p} - (I_y - I_z)qr \\ I_y\dot{q} - (I_z - I_x)rp \\ I_z\dot{r} - (I_x - I_y)pq \end{bmatrix}. \tag{3.2}$$

Here, the quadrotor is symmetric, the inertia matrix is diagonal, and is given by

$$I = \mathrm{diag}(I_x, I_y, I_z) \tag{3.3}$$

where I_x, I_y, and I_z represent the moments of inertia about the body-fixed axes X_b, Y_b, and Z_b, respectively.

Assuming that the angles of the attitude change only slightly near the equilibrium point, we can simplify the change from the motor speed-dependent control inputs to the physical moments acting on the quadrotor airframe and write it as

$$\begin{bmatrix} u_\phi \\ u_\theta \\ u_\psi \end{bmatrix} = \begin{bmatrix} M_x \\ M_y \\ M_z \end{bmatrix} \tag{3.4}$$

Taking into account aerodynamic drag moments and external disturbances affecting the propellers in flight, the disturbance torque vector is characterized as

$$M_d = \begin{bmatrix} -I_r K_1 \dot{\phi} \\ -I_r K_2 \dot{\theta} \\ -I_r K_3 \dot{\psi} \end{bmatrix} \tag{3.5}$$

Remark 2. Approximating the aerodynamic drag torque M_d as a linear function of the angular velocity is a reasonable assumption for quadrotor UAVs operating in hover and moderate flight conditions, where low-frequency rotational damping dominates the aerodynamic behavior. More complex aerodynamic phenomena, including quadratic drag, blade flapping, and wind-induced effects, are lumped into the disturbance term d_i. Because UAVs operate within a finite flight envelope, these unmodeled dynamics and external disturbances can reasonably be assumed to be bounded, that is, $|d_i| \leq \Xi$. Under this assumption, the proposed PFSMC is designed to robustly compensate for these bounded uncertainties, thereby preserving closed-loop stability and tracking performance without requiring an exact model of the high-speed aerodynamic effects.

The dynamics of UAVs are represented as follows [24]:

$$\begin{aligned}
\ddot{\phi} &= \frac{u_\phi}{I_x} - \frac{(I_z - I_y)}{I_x}\dot{\theta}\dot{\psi} - \frac{I_r K_1}{I_x}\dot{\phi} + d_1 \\
\ddot{\theta} &= \frac{u_\theta}{I_y} - \frac{(I_x - I_z)}{I_y}\dot{\phi}\dot{\psi} - \frac{I_r K_2}{I_y}\dot{\theta} + d_2 \\
\ddot{\psi} &= \frac{u_\psi}{I_z} - \frac{(I_y - I_x)}{I_z}\dot{\phi}\dot{\theta} - \frac{I_r K_3}{I_z}\dot{\psi} + d_3
\end{aligned} \tag{3.6}$$

where the following hold:

- ϕ is the roll angle
- θ is the pitch angle
- ψ is the yaw angle
- I_r is the constant of inertia of the propeller
- $I_{x,y,z}$ are the moments of inertia
- $K_{1,2,3}$ are the coefficient of air resistance
- $u_{\phi,\theta,\psi}$ are the control inputs
- d_1, d_2, d_3 are the external disturbances and bounded as $\left|d_{1,2,3}\right| \leq \Xi$ with $\Xi > 0$.

3.2. Control objective

The main goal of the control system is to keep track of and stabilize the roll angle ϕ, pitch angle θ, and yaw angle ψ. This suggests that we desire the real states to move closer to the reference trajectories we seek:

- $\phi \rightarrow \phi_d(t)$
- $\theta \rightarrow \theta_d(t)$
- $\psi \rightarrow \psi_d(t)$

where $\phi_d(t)$, $\theta_d(t)$, and $\psi_d(t)$ represent the target angles. Classical SMC guarantees robustness but is deficient in predefined convergence time. The proposed PFSMC will ensure convergence within a predetermined horizon T_p, irrespective of the initial inaccuracy.

4. Predefined-time fractional-order SMC design

The PFSMC design integrates the principles of sliding manifolds, reaching laws, and Lyapunov analysis. The fundamental concept is to develop a sliding variable whose dynamics are regulated by a nonlinear reaching law that satisfies predefined stability characteristics.

4.1. Tracking error dynamics

The tracking errors are defined as follows:

$$\varsigma_\phi = \phi - \phi_d, \varsigma_\theta = \theta - \theta_d, \varsigma_\psi = \psi - \psi_d$$
$$\dot{\varsigma}_\phi = \dot{\phi} - \dot{\phi}_d, \dot{\varsigma}_\theta = \dot{\theta} - \dot{\theta}_d, \dot{\varsigma}_\psi = \dot{\psi} - \dot{\psi}_d$$
$$\ddot{\varsigma}_\phi = \ddot{\phi} - \ddot{\phi}_d, \ddot{\varsigma}_\theta = \ddot{\theta} - \ddot{\theta}_d, \ddot{\varsigma}_\psi = \ddot{\psi} - \ddot{\psi}_d$$

4.2. Predefined-time fractional-order sliding surface

For $\phi, \theta, and\, \psi$, we construct a sliding surface s such that driving s to zero guarantees the convergence of the tracking error ς and its derivative $\dot{\varsigma}$ to zero. We are going to establish the suggested predefined sliding surfaces as

$$\begin{aligned} s_\phi &= \mathcal{D}^\chi e_\phi + \lambda_{\phi_1}\mathcal{D}^{\chi-1}\left|e_\phi\right|^{1+\beta_\phi} sign(e_\phi) \\ &+\lambda_{\phi_2}\mathcal{D}^{\chi-1}\left|e_\phi\right|^{1-\beta_\phi} sign(e_\phi) \end{aligned} \tag{4.1}$$

$$\begin{aligned} s_\theta &= \mathcal{D}^\chi e_\theta + \lambda_{\theta_1}\mathcal{D}^{\chi-1}|e_\theta|^{1+\beta_\theta} sign(e_\theta) \\ &+\lambda_{\theta_2}\mathcal{D}^{\chi-1}|e_\theta|^{1-\beta_\theta} sign(e_\theta) \end{aligned} \tag{4.2}$$

$$\begin{aligned} s_\psi &= \mathcal{D}^\chi e_\psi + \lambda_{\psi_1}\mathcal{D}^{\chi-1}\left|e_\psi\right|^{1+\beta_\psi} sign(e_\psi) \\ &+\lambda_{\psi_2}\mathcal{D}^{\chi-1}\left|e_\psi\right|^{1-\beta_\psi} sign(e_\psi) \end{aligned} \tag{4.3}$$

where $\lambda_{\phi_1,\theta_1,\psi_1}$ *and* $\lambda_{\phi_2,\theta_2,\psi_2} > 0$, $0 < \beta_{\phi,\theta,\psi}, < 1$, and the fractional-order value is $0 < \chi < 1$. The system dynamics become zero when $s_{\phi,\theta,\psi} = 0$. This indicates that the system is stable and that the error is approaching zero.

Remark 3. Unlike conventional integer-order sliding mode control, which relies solely on the current system states, the proposed fractional-order operator $\mathcal{D}^\chi$ accounts for the past history of the tracking error through its nonlocal memory property. This history-dependent behavior naturally smooths out state transitions near the sliding manifold. Consequently, the proposed PFSMC achieves faster convergence and better tracking precision while mitigating chattering, all without increasing the high-frequency switching control effort.

For brevity, we can rewrite the sliding surface as

$$\begin{aligned} s_i &= \mathcal{D}^\chi e_i + \lambda_{i_1}\mathcal{D}^{\chi-1}|e_i|^{1+\beta_i} sign(e_i) \\ &+\lambda_{i_2}\mathcal{D}^{\chi-1}|e_i|^{1-\beta_i} sign(e_i) \end{aligned} \tag{4.4}$$

where $e_i = \dot{\varsigma}_i + \mu_{i_1}|\varsigma_i|^{1+\gamma_i} sign(\varsigma_i) + \mu_{i_2}|\varsigma_i|^{1-\gamma_i} sign(\varsigma_i)$, $i = \phi, \theta, \psi$, $\mu_{\phi_1,\theta_1,\psi_1}$ *and* $\mu_{\phi_2,\theta_2,\psi_2} > 0$, and $0 < \gamma_{\phi,\theta,\psi}, < 1$.

4.3. PFSMC control design

The objective of SMC is to design a control input that directs the system states to the sliding surface ($s_{\phi,\theta,\psi} = 0$) and thereafter sustains them. This is generally accomplished by control laws consisting of $u_\phi, u_\theta,$ *and* u_ψ that control the angles $\phi, \theta,$ *and* ψ, respectively. The proposed control guarantees that $\dot{s}_{\phi,\theta,\psi} = 0$ when the system is positioned on the sliding surface, whereas the switching control propels the system towards the surface.

The derivative of the sliding surfaces can be obtained as

$$\dot{s}_i = \mathcal{D}^\chi \dot{e}_i + \lambda_{i_1}\mathcal{D}^\chi|e_i|^{1+\beta_i} sign(e_i) + \lambda_{i_2}\mathcal{D}^\chi|e_i|^{1-\beta_i} sign(e_i) \tag{4.5}$$

and the derivative of e_i can be derived as $\dot{e}_i = \ddot{\varsigma}_i + \mu_{i_1}(1+\gamma_i)|\varsigma_i|^{\gamma_i}\dot{\varsigma}_i + \mu_{i_2}(1-\gamma_i)|\varsigma_i|^{-\gamma_i}\dot{\varsigma}_i$.
By substituting $\dot{e}_i$ and $\ddot{\varsigma}_i$ including (3.6) into (4.5), we can have

$$\begin{gathered}\dot{s}_\phi = \mathcal{D}^\chi\begin{pmatrix} \frac{u_\phi}{I_x} - \frac{(I_z-I_y)}{I_x}\dot{\theta}\dot{\psi} - \frac{I_rK_1}{I_x}\dot{\phi} + d_1 - \ddot{\phi}_d \\ +\mu_{\phi_1}(1+\gamma_\phi)\left|\varsigma_\phi\right|^{\gamma_\phi}\dot{\varsigma}_\phi \\ +\mu_{\phi_2}(1-\gamma_\phi)\left|\varsigma_\phi\right|^{-\gamma_\phi}\dot{\varsigma}_\phi \end{pmatrix} \\ +\lambda_{\phi_1}\mathcal{D}^\chi\left|e_\phi\right|^{1+\beta_\phi}sign(e_\phi) + \lambda_{\phi_2}\mathcal{D}^\chi\left|e_\phi\right|^{1-\beta_\phi}sign(e_\phi)\end{gathered} \tag{4.6}$$

$$\begin{gathered}\dot{s}_\theta = \mathcal{D}^\chi\begin{pmatrix} \frac{u_\theta}{I_y} - \frac{(I_x-I_z)}{I_y}\dot{\phi}\dot{\psi} - \frac{I_rK_2}{I_y}\dot{\theta} + d_2 - \ddot{\theta}_d \\ +\mu_{\theta_1}(1+\gamma_\theta)|\varsigma_\theta|^{\gamma_\theta}\dot{\varsigma}_\theta \\ +\mu_{\theta_2}(1-\gamma_\theta)|\varsigma_\theta|^{-\gamma_\theta}\dot{\varsigma}_\theta \end{pmatrix} \\ +\lambda_{\theta_1}\mathcal{D}^\chi|e_\theta|^{1+\beta_\theta}sign(e_\theta) + \lambda_{\theta_2}\mathcal{D}^\chi|e_\theta|^{1-\beta_\theta}sign(e_\theta)\end{gathered} \tag{4.7}$$

$$\begin{gathered}\dot{s}_\psi = \mathcal{D}^\chi\begin{pmatrix} \frac{u_\psi}{I_z} - \frac{(I_y-I_x)}{I_z}\dot{\phi}\dot{\theta} - \frac{I_rK_3}{I_z}\dot{\psi} + d_3 - \ddot{\psi}_d \\ +\mu_{\psi_1}(1+\gamma_\psi)\left|\varsigma_\psi\right|^{\gamma_\psi}\dot{\varsigma}_\psi \\ +\mu_{\psi_2}(1-\gamma_\psi)\left|\varsigma_\psi\right|^{-\gamma_\psi}\dot{\varsigma}_\psi \end{pmatrix} \\ +\lambda_{\psi_1}\mathcal{D}^\chi\left|e_\psi\right|^{1+\beta_\psi}sign(e_\psi) + \lambda_{\psi_2}\mathcal{D}^\chi\left|e_\psi\right|^{1-\beta_\psi}sign(e_\psi)\end{gathered} \tag{4.8}$$

Then, Eqs (4.6)–(4.8) can be rewritten as

$$\begin{gathered}\dot{s}_\phi = \mathcal{D}^\chi\begin{pmatrix} \frac{u_\phi}{I_x} - \Theta_\phi + d_1 - \ddot{\phi}_d + \mu_{\phi_1}(1+\gamma_\phi)\left|\varsigma_\phi\right|^{\gamma_\phi}\dot{\varsigma}_\phi \\ +\mu_{\phi_2}(1-\gamma_\phi)\left|\varsigma_\phi\right|^{-\gamma_\phi}\dot{\varsigma}_\phi \end{pmatrix} \\ +\lambda_{\phi_1}\mathcal{D}^\chi\left|e_\phi\right|^{1+\beta_\phi}sign(e_\phi) + \lambda_{\phi_2}\mathcal{D}^\chi\left|e_\phi\right|^{1-\beta_\phi}sign(e_\phi)\end{gathered} \tag{4.9}$$

where $\Theta_\phi = \frac{(I_z-I_y)}{I_x}\dot{\theta}\dot{\psi} + \frac{I_rK_1}{I_x}\dot{\phi}$,

$$\begin{gathered}\dot{s}_\theta = \mathcal{D}^\chi\begin{pmatrix} \frac{u_\theta}{I_y} - \Theta_\theta + d_2 - \ddot{\theta}_d + \mu_{\theta_1}(1+\gamma_\theta)|\varsigma_\theta|^{\gamma_\theta}\dot{\varsigma}_\theta \\ +\mu_{\theta_2}(1-\gamma_\theta)|\varsigma_\theta|^{-\gamma_\theta}\dot{\varsigma}_\theta \end{pmatrix} \\ +\lambda_{\theta_1}\mathcal{D}^\chi|e_\theta|^{1+\beta_\theta}sign(e_\theta) + \lambda_{\theta_2}\mathcal{D}^\chi|e_\theta|^{1-\beta_\theta}sign(e_\theta)\end{gathered} \tag{4.10}$$

where $\Theta_\theta = \frac{(I_x-I_z)}{I_y}\dot{\phi}\dot{\psi} + \frac{I_rK_2}{I_y}\dot{\theta}$,

$$\begin{gathered}\dot{s}_\psi = \mathcal{D}^\chi\begin{pmatrix} \frac{u_\psi}{I_z} - \Theta_\psi + d_3 - \ddot{\psi}_d + \mu_{\psi_1}(1+\gamma_\psi)\left|\varsigma_\psi\right|^{\gamma_\psi}\dot{\varsigma}_\psi \\ +\mu_{\psi_2}(1-\gamma_\psi)\left|\varsigma_\psi\right|^{-\gamma_\psi}\dot{\varsigma}_\psi \end{pmatrix} \\ +\lambda_{\psi_1}\mathcal{D}^\chi\left|e_\psi\right|^{1+\beta_\psi}sign(e_\psi) + \lambda_{\psi_2}\mathcal{D}^\chi\left|e_\psi\right|^{1-\beta_\psi}sign(e_\psi)\end{gathered} \tag{4.11}$$

where $\Theta_\psi = \frac{(I_y-I_x)}{I_z}\dot{\theta}\dot{\phi} + \frac{I_rK_3}{I_z}\dot{\psi}$. Then Eqs (4.9)–(4.11) can be represented as

$$\begin{gathered}\dot{s}_i = \mathcal{D}^\chi\begin{pmatrix} \frac{u_i}{I_p} - \Theta_i + d_i - \ddot{i}_d + \mu_{i_1}(1+\gamma_i)|\varsigma_i|^{\gamma_i}\dot{\varsigma}_i \\ +\mu_{i_2}(1-\gamma_i)|\varsigma_i|^{-\gamma_i}\dot{\varsigma}_i \end{pmatrix} \\ +\lambda_{i_1}\mathcal{D}^\chi|e_i|^{1+\beta_i}sign(e_i) + \lambda_{i_2}\mathcal{D}^\chi|e_i|^{1-\beta_i}sign(e_i)\end{gathered} \tag{4.12}$$

where $p = x, y, z$.

The proposed control scheme for the roll, pitch, and yaw angles of the UAV dynamics (3.6) based on the proposed sliding surfaces is given as

$$u_i = I_p \begin{pmatrix} \ddot{i}_d + \Theta_i - \Xi sign(s_i) \\ -\mu_{i_1}(1+\gamma_i)|\varsigma_i|^{\gamma_i}\dot{\varsigma}_i - \mu_{i_2}(1-\gamma_i)|\varsigma_i|^{-\gamma_i}\dot{\varsigma}_i \\ -\lambda_{i_1}|e_i|^{1+\beta_i} sign(e_i) - \lambda_{i_2}|e_i|^{1-\beta_i} sign(e_i) \\ -k_{i_1}\mathcal{D}^{-\chi}|s_i|^{1+\frac{\alpha_i}{2}} sign(s_i) \\ -k_{i_2}\mathcal{D}^{-\chi}|s_i|^{1-\frac{\alpha_i}{2}} sign(s_i) \end{pmatrix} \tag{4.13}$$

where $|\varsigma_i|^{-\gamma_i} = 0 \; if \; \varsigma_i = 0$. k_{i1} and k_{i2} and $0 < \alpha_i < 1$ are known positive constants. The proposed block diagram is shown in Figure 2.

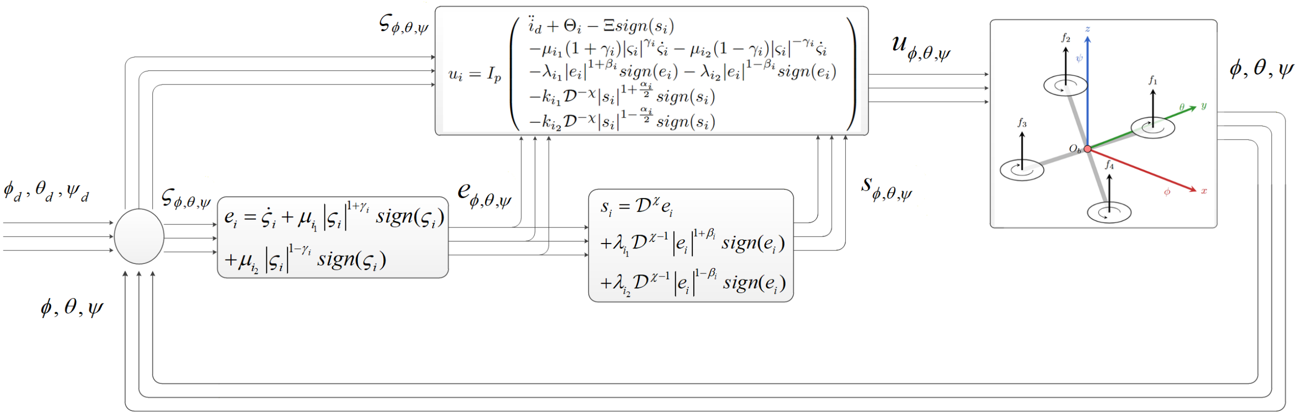

Figure 2. Proposed block diagram.

5. Stability analysis

This section presents the stability of each individual sliding surface. By guaranteeing that each sliding surface s_ϕ, s_θ, and s_ψ approaches zero within a predefined timeframe, while maintaining the system states on these surfaces, the tracking errors for ϕ, θ, and ψ (together with their derivatives) will decrease to zero. This indicates that the UAV will effectively monitor the specified angular trajectories and maintain stability in its angles.

5.1. Stability analysis of the sliding surface

The following Lyapunov candidate is selected as

$$V = \frac{1}{2}\sum_{i=1}^{3} s_i^2 \tag{5.1}$$

The derivative of V is given as

$$\dot{V} = \sum_{i=1}^{3} s_i \dot{s}_i \tag{5.2}$$

Substitution of (4.12) into $\dot{V}$ gives

$$\dot{V} = \sum_{i=1}^{3} s_i \begin{pmatrix} \mathcal{D}^{\chi} \begin{pmatrix} \frac{u_i}{I_p} - \Theta_i + d_i - \dddot{i}_d \\ +\mu_{i_1}(1+\gamma_i)|\varsigma_i|^{\gamma_i}\dot{\varsigma}_i \\ +\mu_{i_2}(1-\gamma_i)|\varsigma_i|^{-\gamma_i}\dot{\varsigma}_i \end{pmatrix} \\ +\lambda_{i_1}\mathcal{D}^{\chi}|e_i|^{1+\beta_i} sign(e_i) \\ +\lambda_{i_2}\mathcal{D}^{\chi}|e_i|^{1-\beta_i} sign(e_i) \end{pmatrix} \tag{5.3}$$

Substitution of (4.13) into $\dot{V}$ yields

$$\dot{V} = \sum_{i=1}^{3} s_i \begin{pmatrix} \mathcal{D}^{\chi} \begin{pmatrix} \begin{pmatrix} \dddot{i}_d + \Theta_i - \Xi sign(s_i) \\ -\mu_{i_1}(1+\gamma_i)|\varsigma_i|^{\gamma_i}\dot{\varsigma}_i \\ -\mu_{i_2}(1-\gamma_i)|\varsigma_i|^{-\gamma_i}\dot{\varsigma}_i \\ -\lambda_{i_1}|e_i|^{1+\beta_i} sign(e_i) \\ -\lambda_{i_2}|e_i|^{1-\beta_i} sign(e_i) \\ -k_{i_1}\mathcal{D}^{-\chi}|s_i|^{1+\frac{\alpha_i}{2}} sign(s_i) \\ -k_{i_2}\mathcal{D}^{-\chi}|s_i|^{1-\frac{\alpha_i}{2}} sign(s_i) \end{pmatrix} \\ -\Theta_i + d_i - \dddot{i}_d + \mu_{i_1}(1+\gamma_i)|\varsigma_i|^{\gamma_i}\dot{\varsigma}_i \\ +\mu_{i_2}(1-\gamma_i)|\varsigma_i|^{-\gamma_i}\dot{\varsigma}_i \end{pmatrix} \\ +\lambda_{i_1}\mathcal{D}^{\chi}|e_i|^{1+\beta_i} sign(e_i) \\ +\lambda_{i_2}\mathcal{D}^{\chi}|e_i|^{1-\beta_i} sign(e_i) \end{pmatrix} \tag{5.4}$$

By solving the above equation using bounded conditions of disturbances, we obtain

$$\dot{V} \leq \sum_{i=1}^{3} s_i \left(-k_{i_1}|s_i|^{1+\frac{\alpha_i}{2}} sign(s_i) - k_{i_2}|s_i|^{1-\frac{\alpha_i}{2}} sign(s_i) \right) \tag{5.5}$$

$$\Rightarrow \dot{V} \leq -k_1 \sum_{i=1}^{3} \left(|s_i|^2\right)^{\frac{2+\frac{\alpha_i}{2}}{2}} - k_2 \sum_{i=1}^{3} \left(|s_i|^2\right)^{\frac{2-\frac{\alpha_i}{2}}{2}} \tag{5.6}$$

where $k_1 = \min(k_{i_1})$ and $k_2 = \min(k_{i_2})$. Using Lemma 2, it can be expressed as

$$\dot{V} \leq -k_1 3^{-\frac{\alpha_i}{4}} \left(\sum_{i=1}^{3} |s_i|^2\right)^{\frac{4+\alpha_i}{4}} - k_2 \left(\sum_{i=1}^{3} |s_i|^2\right)^{\frac{4-\alpha_i}{4}} \tag{5.7}$$

Then, it can be represented as

$$\dot{V} \leq -k_1 3^{-\frac{\alpha_i}{4}} 2^{1+\frac{\alpha_i}{4}} V^{1+\frac{\alpha_i}{4}} - k_2 2^{1-\frac{\alpha_i}{4}} V^{1-\frac{\alpha_i}{4}} \tag{5.8}$$

Using Lemma 1, the settling time can be formulated as

$$T_{r_i} = \frac{\pi}{\alpha_i \sqrt{k_1 k_2 3^{-\frac{\alpha_i}{4}}}}$$

Because $k_1 > 0$ and $k_2 > 0$, the sliding surface s_i remains stable for a predefined time, and the error ς_i converges to zero.

5.2. Stability analysis of the tracking error

When $s_{\phi,\theta,\psi} = 0$, the error dynamics are simplified to a stable reduced-order manifold. During this phase, the high-order nonlinearities in the UAV dynamics are eliminated, and the system's behavior is entirely controlled by the sliding surface parameters, ensuring that the tracking errors converge to the origin. To investigate the stability of this condition, a Lyapunov candidate function is selected as follows:

$$\bar{V} = \bar{V}_{\varsigma} + \bar{V}_{e} = \frac{1}{2}\sum_{i=1}^{3}\varsigma_i^2 + \frac{1}{2}\sum_{i=1}^{3}e_i^2 \tag{5.9}$$

The derivative of $\bar{V}$ can be obtained as

$$\dot{\bar{V}} = \sum_{i=1}^{3}\varsigma_i\dot{\varsigma}_i + \sum_{i=1}^{3}e_i\dot{e}_i \tag{5.10}$$

Then, it can be expressed as

$$\dot{\bar{V}} = \sum_{i=1}^{3}\varsigma_i\dot{\varsigma}_i + \sum_{i=1}^{3}e_i\mathcal{D}^{1-\chi}(\mathcal{D}^{\chi}e_i) \tag{5.11}$$

When $s_i = 0$, and $e_i = 0$ from (4.4), we can have respectively: $\mathcal{D}^{\chi}e_i = -\lambda_{i_1}\mathcal{D}^{\chi-1}|e_i|^{1+\beta_i}sign(e_i) - \lambda_{i_2}\mathcal{D}^{\chi-1}|e_i|^{1-\beta_i}sign(e_i)$ and $\dot{\varsigma}_i = -\mu_{i_1}|\varsigma_i|^{1+\gamma_i}sign(\varsigma_i) - \mu_{i_2}|\varsigma_i|^{1-\gamma_i}sign(\varsigma_i)$. By substituting $\mathcal{D}^{\chi}e_i$ and $\dot{\varsigma}_i$ into (5.11), we write

$$\begin{aligned}
\dot{\bar{V}} &= \sum_{i=1}^{3}\varsigma_i\begin{pmatrix} -\mu_{i_1}|\varsigma_i|^{1+\gamma_i}sign(\varsigma_i) \\ -\mu_{i_2}|\varsigma_i|^{1-\gamma_i}sign(\varsigma_i)\end{pmatrix} \\
&+ \sum_{i=1}^{3}e_i\mathcal{D}^{1-\chi}\begin{pmatrix} -\lambda_{i_1}\mathcal{D}^{\chi-1}|e_i|^{1+\beta_i}sign(e_i) \\ -\lambda_{i_2}\mathcal{D}^{\chi-1}|e_i|^{1-\beta_i}sign(e_i)\end{pmatrix} \\
&= -\mu_{i_1}\sum_{i=1}^{3}|\varsigma_i|^{2+\gamma_i} - \mu_{i_2}\sum_{i=1}^{3}|\varsigma_i|^{2-\gamma_i} \\
&-\lambda_{i_1}\sum_{i=1}^{3}|e_i|^{2+\beta_i} - \lambda_{i_2}\sum_{i=1}^{3}|e_i|^{2-\beta_i}
\end{aligned} \tag{5.12}$$

It can be rewritten as

$$\begin{aligned}
\dot{\bar{V}} &= -\mu_{i_1}\sum_{i=1}^{3}\left(|\varsigma_i|^2\right)^{\frac{2+\gamma_i}{2}} - \mu_{i_2}\sum_{i=1}^{3}\left(|\varsigma_i|^2\right)^{\frac{2-\gamma_i}{2}} \\
&-\lambda_{i_1}\sum_{i=1}^{3}\left(|e_i|^2\right)^{\frac{2+\beta_i}{2}} - \lambda_{i_2}\sum_{i=1}^{3}\left(|e_i|^2\right)^{\frac{2-\beta_i}{2}}
\end{aligned} \tag{5.13}$$

Using Lemma 2, it can be computed as

$$\begin{aligned}
\dot{\bar{V}} &\leq -\mu_1 3^{-\frac{\gamma_i}{2}}\left(\sum_{i=1}^{3}|\varsigma_i|^2\right)^{1+\frac{\gamma_i}{2}} - \mu_2\left(\sum_{i=1}^{3}|\varsigma_i|^2\right)^{1-\frac{\gamma_i}{2}} \\
&-\lambda_1 3^{-\frac{\beta_i}{2}}\left(\sum_{i=1}^{3}|e_i|^2\right)^{1+\frac{\beta_i}{2}} - \lambda_2\left(\sum_{i=1}^{3}|e_i|^2\right)^{1-\frac{\beta_i}{2}}
\end{aligned} \tag{5.14}$$

where $\mu_1 = \min(\mu_{i_1})$, $\mu_2 = \min(\mu_{i_2})$, $\lambda_1 = \min(\lambda_{i_1})$, and $\lambda_2 = \min(\lambda_{i_2})$. Using (5.9), this can be expressed as

$$\begin{aligned}
\dot{\bar{V}} &\leq -\mu_1 3^{-\frac{\gamma_i}{2}}2^{1+\frac{\gamma_i}{2}}\bar{V}_{\varsigma}^{1+\frac{\gamma_i}{2}} - \mu_2 2^{1-\frac{\gamma_i}{2}}\bar{V}_{\varsigma}^{1-\frac{\gamma_i}{2}} \\
&-\lambda_1 3^{-\frac{\beta_i}{2}}2^{1+\frac{\beta_i}{2}}\bar{V}_{e}^{1+\frac{\beta_i}{2}} - \lambda_2 2^{1-\frac{\beta_i}{2}}\bar{V}_{e}^{1-\frac{\beta_i}{2}}
\end{aligned} \tag{5.15}$$

According to Lemma 1, we can compute the settling time as

$$T_{s_i} = \frac{\pi}{2\gamma_i \sqrt{\mu_1 \mu_2 3^{-\frac{\gamma_i}{2}}}} + \frac{\pi}{2\beta_i \sqrt{\lambda_1 \lambda_2 3^{-\frac{\beta_i}{2}}}} \tag{5.16}$$

It ensures convergence of both ς_i and e_i within the predefined time T_{s_i}. Hence, predefined-time stability of the closed-loop UAV system is guaranteed.

Remark 4. In the proposed stability analysis, the overall settling time of the tracking system is conservatively bounded by the maximum of the channel-wise settling-time upper bounds, given by $T_{\max} = \max_{i\in\{1,2,3\}} (T_{r_i} + T_{s_i})$, where T_{r_i} denotes the analytical upper bound of the reaching phase, and $T_{s_i} = T_{\varsigma_i} + T_{e_i}$ represents the analytical upper bound of the sliding-phase convergence. Consequently, the closed-loop settling time satisfies

$$T_{\text{actual}} \leq T_{\max} = \max_{i\in\{1,2,3\}} \left(T_{r_i} + T_{s_i}\right). \tag{5.17}$$

Here, T_{actual} denotes the actual settling time of the closed-loop system. Although the analytical bound $T_{\max}$ may be conservative, it provides a rigorous and verifiable worst-case estimate of the convergence time. Furthermore, expressing the settling time as the sum of independently derived upper bounds avoids the analytical complexity associated with directly solving Lyapunov inequalities involving multiple fractional-order terms with different exponents.

6. Simulation results

To assess the efficacy of the proposed predefined-time fractional-order sliding mode control (PFSMC), numerical simulations were performed in MATLAB/Simulink. Moreover, the FOMCON toolbox has been used to implement fractional-order control. A conventional quadrotor design, featuring four identical rotors arranged in a cross formation, was examined. The proposed scheme is compared with finite-time SMC (FTSMC) [25], fixed-time SMC (FxSMC) [26], and fractional FxSMC (FFxSMC) [27].

6.1. Parameter setup and performance evaluation

The parameters of the dynamical model in (3.6) are presented in Table 1. Moreover, the parameters of the proposed method utilized in the simulations are listed in Table 2. Aerodynamic drag coefficients are selected to model realistic rotational damping. Additionally, the target tracking values for the quadrotor's attitude are defined as $[\phi_d; \theta_d; \psi_d] = [\sin(t)+1; \cos(t)-0.5; 0.1t]$. The external disturbances are applied as $d_{1,2,3} = 0.1\sin(t) + 0.4$.

Table 1. Quadrotor parameters used in simulation.

Parameter	Value	Units
I_x	2.5	$kg.m^2$
I_y	1.25	$kg.m^2$
I_z	2.5	$kg.m^2$
I_r	1	$kg.m^2$
K_1	0.2	$N.s.m^{-1}$
K_2	0.2	$N.s.m^{-1}$
K_3	0.2	$N.s.m^{-1}$

Table 2. Proposed control parameters used in simulation.

Parameter	Value	Parameter	Value
$\lambda_{\phi_{1,2}}$	10	α_ϕ	0.9
$\lambda_{\theta_{1,2}}$	10	α_θ	0.9
$\lambda_{\psi_{1,2}}$	10	α_ψ	0.9
$k_{\phi_{1,2}}$	15	β_ϕ	0.8
$k_{\theta_{1,2}}$	15	β_θ	0.8
$k_{\psi_{1,2}}$	15	β_ψ	0.8
$\mu_{\phi_{1,2}}$	4	γ_ϕ	0.3
$\mu_{\theta_{1,2}}$	4	γ_θ	0.3
$\mu_{\psi_{1,2}}$	4	γ_ψ	0.3

Figures 3–5 illustrate the trajectory tracking of the proposed controller. The PFSMC attained convergence precisely within the predefined time frame. In Figure 6, a comparison of helical paths for pitch, roll, and yaw is shown. Figures 7–9 depict the tracking errors across all angles, demonstrating rapid convergence and minimal errors. Figures 10–12 illustrate the control input, demonstrating that the PFSMC produced more refined control signals and that its reduced chattering enhances its compatibility with the system. Moreover, the quantitative analysis of the proposed and compared control schemes is presented as the root mean square error (RMSE) in Table 3. This clearly shows that the proposed approach yields smaller tracking errors than the compared methods.

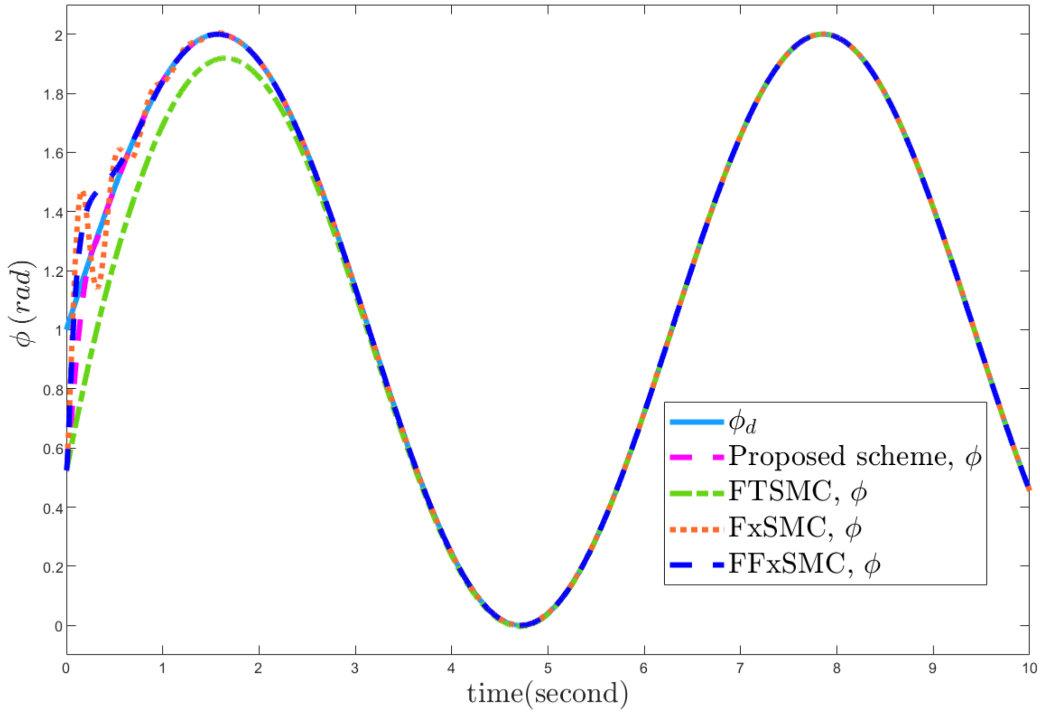

Figure 3. Roll angle tracking.

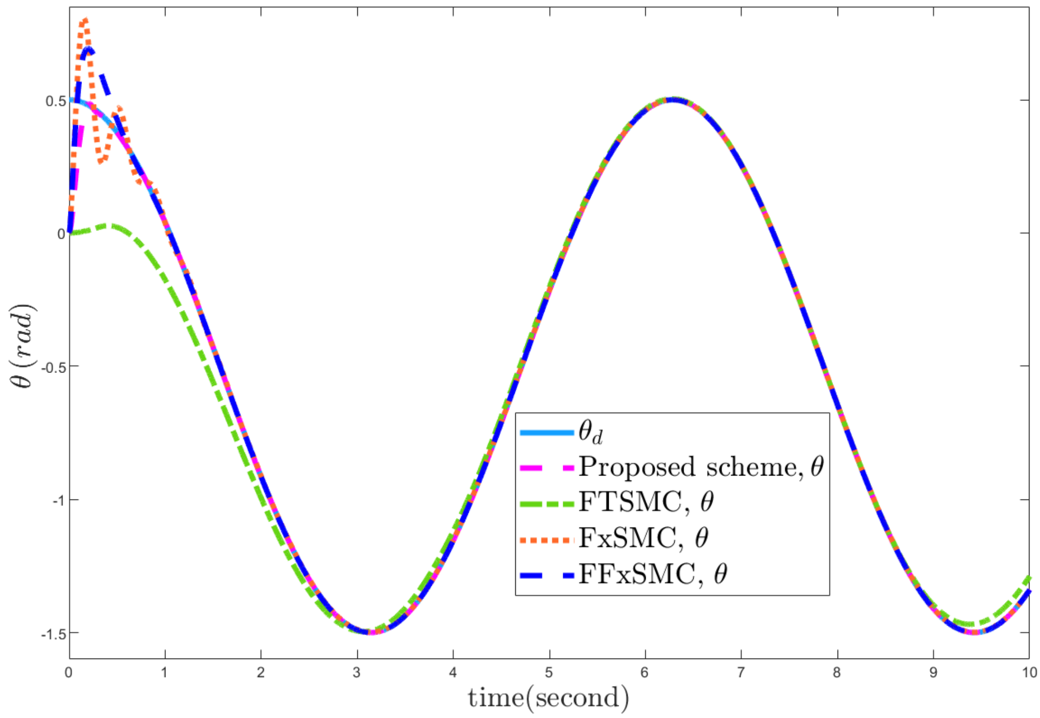

Figure 4. Pitch angle tracking.

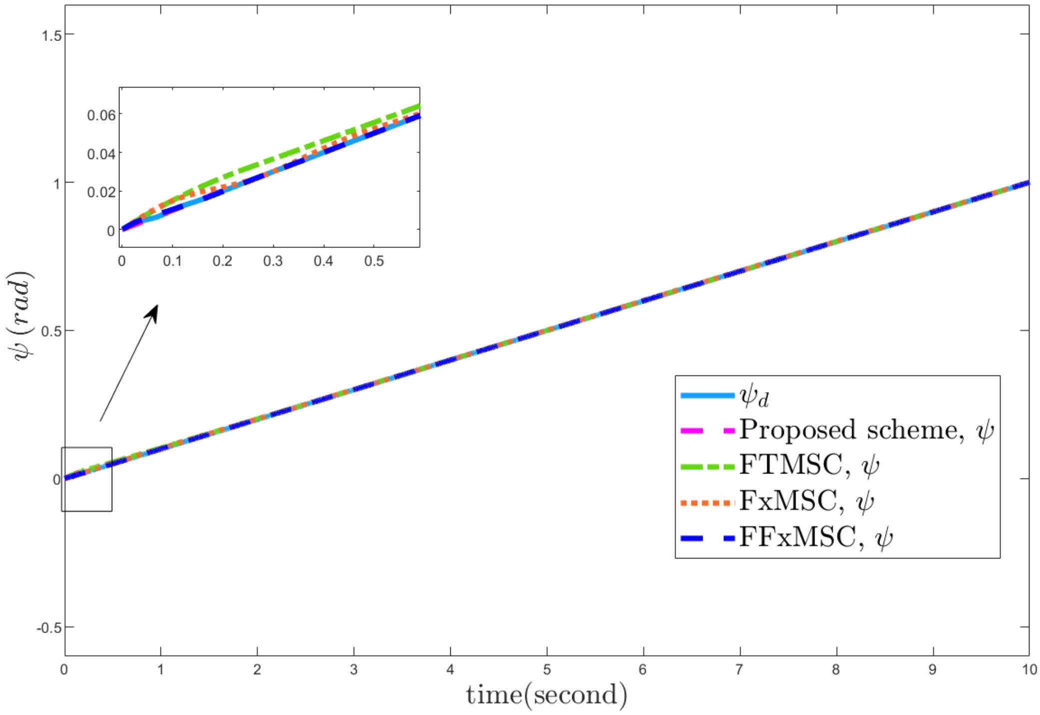

Figure 5. Yaw angle tracking.

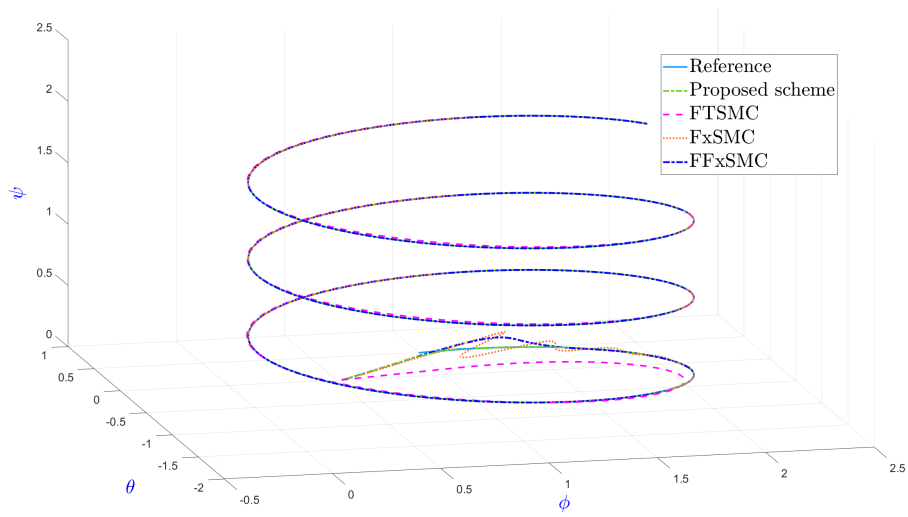

Figure 6. A comparison of complex helical paths for pitch, roll, and yaw with FTSMC.

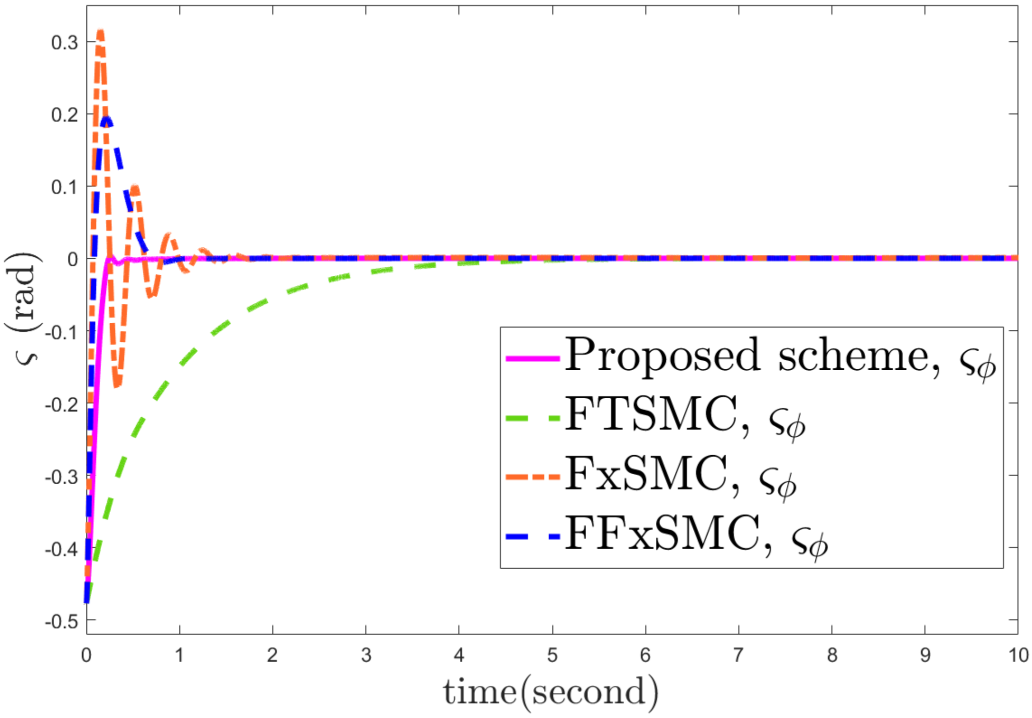

Figure 7. Roll tracking errors.

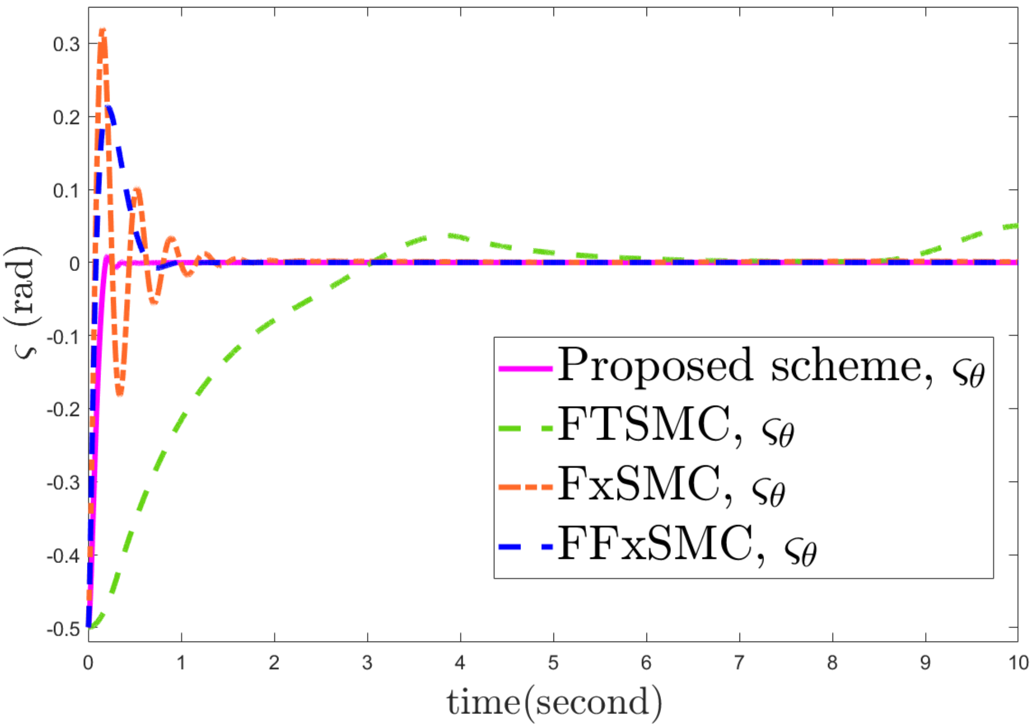

Figure 8. Pitch tracking errors.

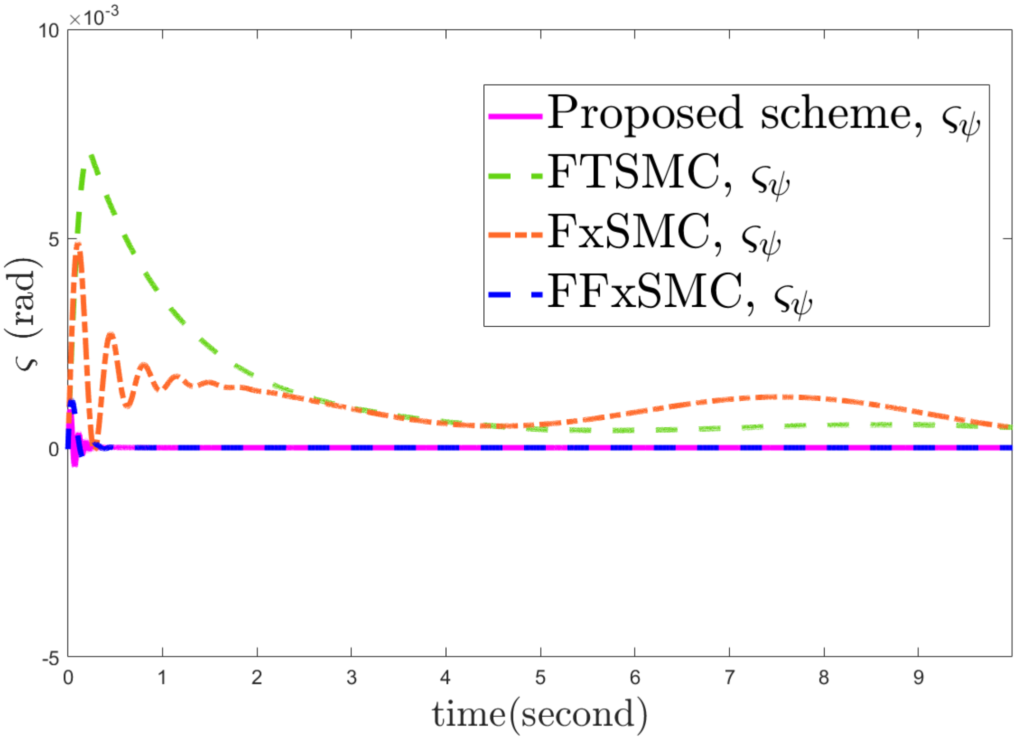

Figure 9. Yaw tracking errors.

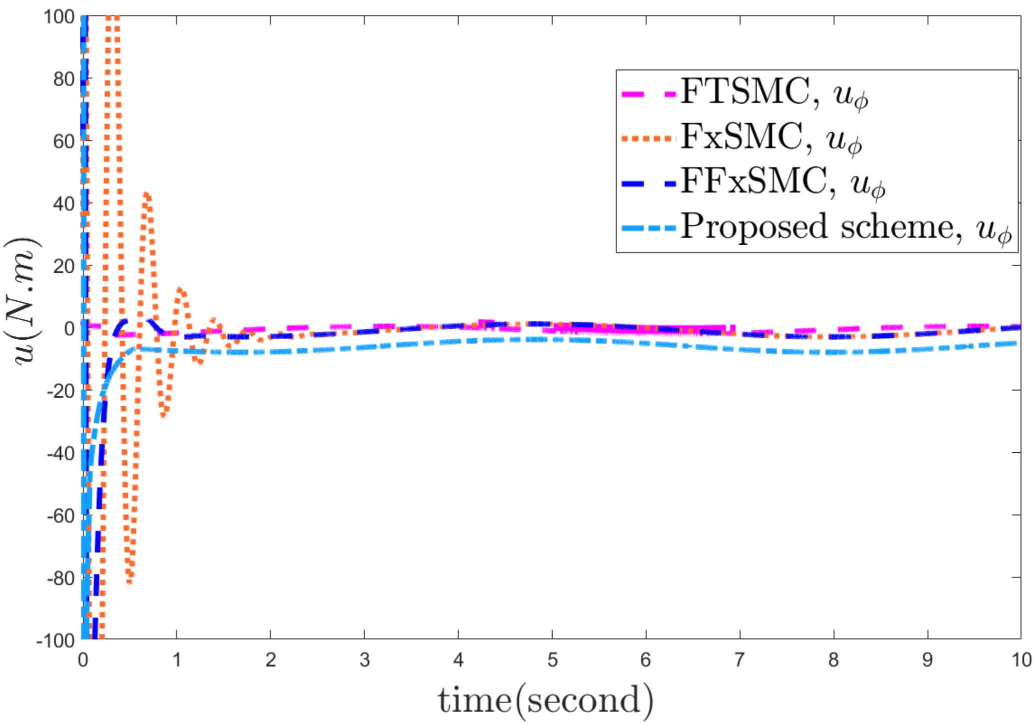

Figure 10. Roll control inputs.

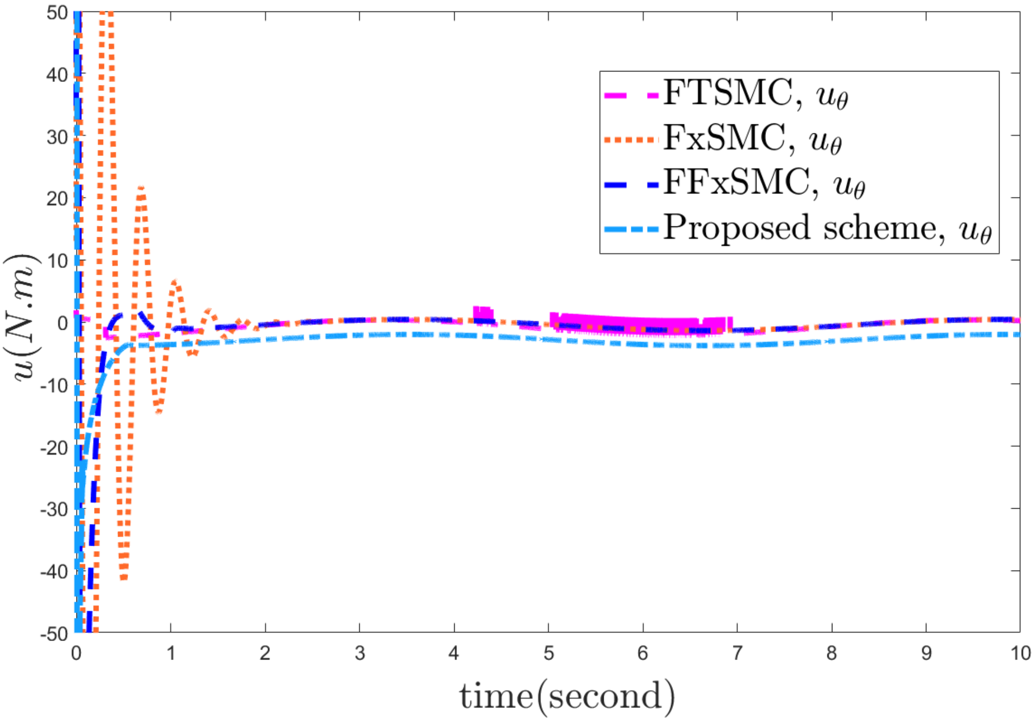

Figure 11. Pitch control inputs.

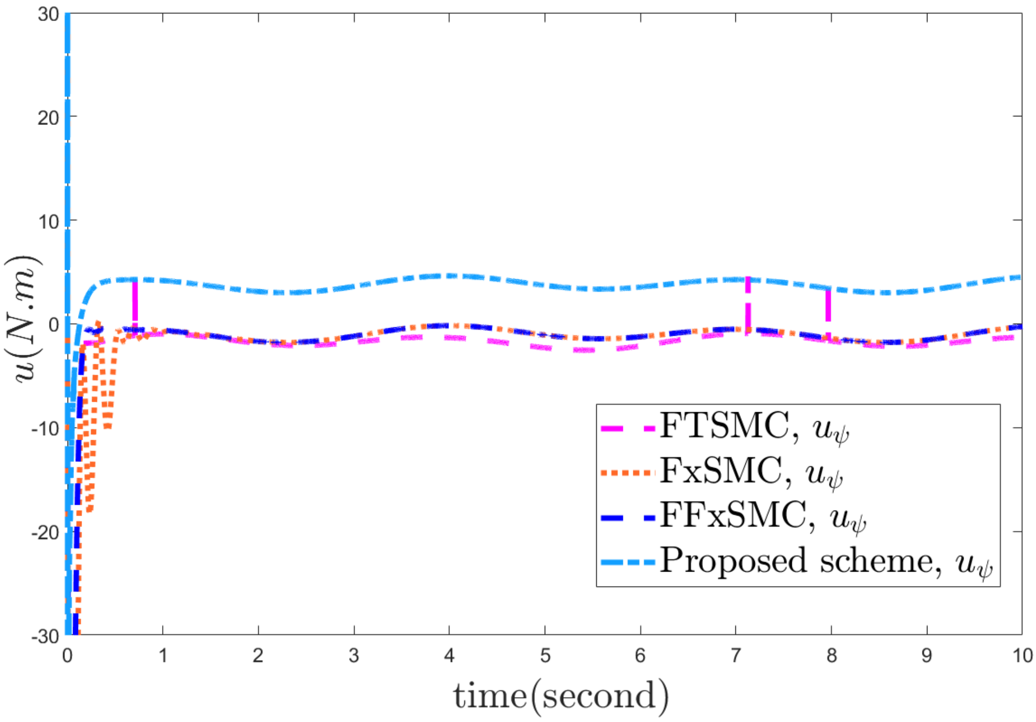

Figure 12. Yaw control inputs.

Table 3. RMS error of proposed, FTSMC, FxSMC, and FFxSMC schemes.

	Proposed scheme	FTSMC	FxSMC	FFxSMC
$\varsigma_{\phi,RMSE}$	0.0250	0.0470	0.0315	0.0279
$\varsigma_{\theta,RMSE}$	0.0265	0.0671	0.0327	0.0296
$\varsigma_{\psi,RMSE}$	7.6949×10^{-6}	1.7562×10^{-4}	$9.7899\times10-4$	$6.3645\times10-5$

The comparative simulation results show that the proposed PFSMC uniquely guarantees tracking convergence within a predefined time, ensuring a deterministic settling time. Furthermore, although all evaluated schemes maintained system stability under the applied disturbances, the PFSMC demonstrated superior robustness by achieving the lowest tracking errors. It also significantly mitigated chattering, resulting in much smoother control inputs.

6.2. Computational overhead and profiling analysis

Standard integer-order sliding mode controllers calculate control laws using only current states with a fixed number of operations per step. In contrast, fractional-order architectures such as the proposed PFSMC and the FFxSMC baseline introduce history-dependent operators $\mathcal{D}^{\chi}$. Simulating these operators using the fractional-order toolbox incurs additional memory allocation and calculations at each sampling interval.

To measure this penalty, we tested the proposed PFSMC alongside FTSMC, FxSMC, and FFxSMC schemes under identical conditions using the Simulink Profiler. The simulation ran for 10 seconds using a fixed-step Runge–Kutta solver with a step size of $T_s = 0.001$s. Throughout the execution window, the profiler recorded exactly 110,015 cumulative block invocations across all evaluated control loops, reflecting the total major and minor integration steps executed by the simulation. The data shows that the proposed PFSMC and the FFxSMC baseline require longer total execution times than the integer-order methods (FTSMC and FxSMC). This is expected, given the extra steps required to review historical tracking data. However, the absolute overhead between the two fractional schemes is minimal, with the proposed PFSMC showing only a 2% increase in total time over the FFxSMC baseline.

Notably, the controller's self-time, the time spent strictly running the core algorithm rather than the block wrappers, is 0.613s for the PFSMC compared to 0.704s for FFxSMC. This indicates that the minor difference in total execution time stems from simulation environment wrapper overhead rather than a heavier algorithmic workload, demonstrating that the proposed predefined-time structure introduces a computational profile entirely comparable to existing fractional-order schemes.

7. Conclusions

This research has developed and evaluated a PFSMC method for UAV systems. Starting with a nonlinear model of quadrotor dynamics, we formulated a predefined-time sliding manifold and control rule, and we demonstrated convergence using Lyapunov stability theory. Comparative simulations of FTSMC, FxSMC, and FFxSMC in the presence of air resistance validated the superiority of PFSMC, particularly in terms of predetermined timing, robustness, and smooth control inputs. The results indicate that PFSMC is well-suited to UAV models that require both robustness and stability.

Current limitations rely on prior disturbance bounds, which may limit robustness in unmodeled environments. Future work will address this by integrating adaptive control with the predefined-time fractional-order framework to autonomously reject unknown disturbances without prior information.

Author contributions

Saim Ahmed: Conceptualization, Investigation, Methodology, Formal analysis, Writing–original draft, Writing–review & editing, Funding; Ahmad Taher Azar: Conceptualization, Investigation, Formal analysis, Writing–review & editing, Supervision, Funding; Rozaimi Ghazali: Formal analysis, Writing–review & editing, Supervision, Funding.

Use of Generative-AI tools declaration

During the preparation of this manuscript, the authors did not use any AI tools for the original manuscript preparation; however, they have used Grammarly Premium for language editing, grammar checking, and improving its clarity and readability.

Acknowledgments

This study was supported by a research grant provided by the Research, Development, and Innovation Authority (RDIA), Kingdom of Saudi Arabia, with Grant No. 13382-psu-2023-PSNU-R-3-1-EI-. The authors would like to acknowledge the support of Prince Sultan University, Riyadh, Saudi Arabia, in paying the article processing charges of this publication. In addition, this research is supported by the Automated Systems and Computing Lab (ASCL), Prince Sultan University, Riyadh, Saudi Arabia. The authors would like to express their gratitude to Universiti Teknikal Malaysia Melaka and the Ministry of Higher Education (MoHE) for their support.

Conflict of interest

The authors declare no conflict of interest.

References

1. S. Gupte, P. I. T. Mohandas, J. M. Conrad, A survey of quadrotor unmanned aerial vehicles, In: *2012 Proceedings of IEEE Southeastcon*, Orlando, FL, USA, 2012, 1–6. https://doi.org/10.1109/SECon.2012.6196930
2. J. Kim, S. A. Gadsden, S. A. Wilkerson, A comprehensive survey of control strategies for autonomous quadrotors, *Canadian Journal of Electrical and Computer Engineering*, **43** (2020), 3–16. https://doi.org/10.1109/CJECE.2019.2920938
3. K. Shao, K. Huang, S. Zhen, H. Sun, R. Yu, A novel approach for trajectory tracking control of an under-actuated quad-rotor UAV, *IEEE/CAA J. Automatic. Sin.*, **11** (2024), 2030–2032. https://doi.org/10.1109/JAS.2016.7510238

4. K. Saber, M. Elarkam, N. Nourreddine, A. Zahir, Performance comparison of PID, LQR, and H∞ controllers for quadrotor attitude and altitude control, *Journal Européen des Systèmes Automatisés*, **58** (2025), 2389–2404. https://doi.org/10.18280/jesa.581116

5. A. S. Elkhatem, S. N. Engin, Robust LQR and LQR-PI control strategies based on adaptive weighting matrix selection for a UAV position and attitude tracking control, *Alex. Eng. J.*, **61** (2022), 6275–6292. https://doi.org/10.1016/j.aej.2021.11.057

6. V. I. Utkin, Sliding mode control design principles and applications to electric drives, *IEEE Trans. Ind. Electron.*, **40** (1993), 23–36. https://doi.org/10.1109/41.184818

7. H. Khan, J. Alzabut, J. Gómez-Aguilar, P. Agarwal, Piecewise mabc fractional derivative with an application, *AIMS Math.*, **8** (2023), 24345–24366. https://doi.org/10.3934/math.20231241

8. H. Khan, H. B. Amer, R. Latif, W. F. Alfwzan, R. Thinakaran, Investigation of radioisotopes population dynamics by the help of modeling and artificial intelligence, *Fractals*, **34** (2026), 2640035. https://doi.org/10.1142/S0218348X26400359

9. Z. Li, L. Liu, S. Dehghan, Y. Chen, D. Xue, A review and evaluation of numerical tools for fractional calculus and fractional order controls, *Int. J. Control*, **90** (2017), 1165–1181. https://doi.org/10.1080/00207179.2015.1124290

10. S. Ahmed, A. T. Azar, Predefined-time fractional-order terminal smc for robot dynamics, *IJOCTA*, **15** (2025), 426–434. https://doi.org/10.36922/IJOCTA025060020

11. O. Mofid, S. Mobayen, Robust fractional-order sliding mode tracker for quad-rotorUAVs: event-triggered adaptive backstepping approach under disturbance and uncertainty, *Aerosp. Sci. Technol.*, **146** (2024), 108916. https://doi.org/10.1016/j.ast.2024.108916

12. I. Podlubny, *Fractional differential equations: an introduction to fractional derivatives, fractional differential equations, to methods of their solution and some of their applications*, New York: Academic press, 1999. https://doi.org/10.1016/S0076-5392(99)X8001-5

13. S. P. Bhat, D. S. Bernstein, Finite-time stability of continuous autonomous systems, *SIAM J. Control Optim.*, **38** (2000), 751–766. https://doi.org/10.1137/S0363012997321358

14. T.-F. Ding, K.-T. Xu, M.-F. Ge, J. H. Park, C.-D. Liang, Fast fixed-time output multi-formation tracking of networked autonomous surface vehicles: a mathematical induction method, *IEEE Trans. Veh. Technol.*, **72** (2023), 5769–5781. https://doi.org/10.1109/TVT.2022.3233887

15. X. Jin, J. Jiang, J. Qin, W. X. Zheng, M. Gao, Observer-based fixed-time-synchronized control for uncertain euler–lagrange systems with bias–actuator faults, *IEEE Trans. Cybernetics*, **55** (2025), 3811–3824. https://doi.org/10.1109/TCYB.2025.3576397

16. M. Gao, L. Ding, X. Jin, ELM-based adaptive faster fixed-time control of robotic manipulator systems, *IEEE Trans. Neur. Net. Lear.*, **34** (2023), 4646–4658. https://doi.org/10.1109/TNNLS.2021.3116958

17. T.-F. Ding, M.-F. Ge, Z.-W. Liu, M. Chi, C. K. Ahn, Cluster time-varying formation-containment tracking of networked robotic systems via hierarchical prescribed-time eso-based control, *IEEE Trans. Netw. Sci. Eng.*, **11** (2024), 566–577, https://doi.org/10.1109/TNSE.2023.3302011

18. T.-F. Ding, M.-F. Ge, C. Xiong, Z.-W. Liu, G. Ling, Prescribed-time formation tracking of second-order multi-agent networks with directed graphs, *Automatica*, **152** (2023), 110997. https://doi.org/10.1016/j.automatica.2023.110997

19. K. Shao, J. Zheng, Predefined-time sliding mode control with prescribed convergent region, *IEEE/CAA J. Automatic. Sin.*, **9** (2022), 934–936. https://doi.org/10.1109/JAS.2022.105575

20. S. Ahmed, A. T. Azar, W. El-Shafai, Adaptive predefined-time fractional terminal sliding mode control for robotic dynamic systems, *J. Math. Comput. Sci.*, **41** (2026), 550–563. https://doi.org/10.22436/jmcs.041.04.06

21. A. J. Muñoz-Vázquez, J. D. Sánchez-Torres, S. Gutiérrez-Alcalá, E. Jiménez-Rodríguez, A. G. Loukianov, Predefined-time robust contour tracking of robotic manipulators, *J. Franklin I.*, **356** (2019), 2709–2722. https://doi.org/10.1016/j.jfranklin.2019.01.041

22. S. Ahmed, A. T. Azar, Adaptive pd sliding mode control for robot dynamics using predefined-time approach, *Int. J. Dynam. Control*, **13** (2025), 100. https://doi.org/10.1007/s40435-025-01603-y

23. M. Alhazmi, S. M. Mirgani, A. Aljohani, S. Saber, Numerical simulation of a fractional glucose-insulin model via successive approximation and abm schemes, *AIMS Math.*, **10** (2025), 22817–22849. https://doi.org/10.3934/math.20251014

24. J. Dou, D. Xie, Y. Wu, T. Zhang, A non-singular sliding mode controller for quadrotor attitude with predefined time disturbance observer, *Adv. Mech. Eng.*, **17** (2025), 1–14. https://doi.org/10.1177/16878132251372787

25. I. H. Imran, D. F. Kurtulus, T. Kouser, A. M. Memon, L. M. Alhems, S. Goli, Finite time sliding mode control for chattering reduction in unmanned aerial vehicles with dynamic payloads, *IEEE Access*, **13** (2025), 143196–143209. https://doi.org/10.1109/ACCESS.2025.3598131

26. A. K. Kamath, N. T. Chan, M. Feroskhan, Fixed-time fractional-order sliding mode control for image-based visual servoing of hexarotor, In: *2024 International conference on unmanned aircraft systems (ICUAS)*. Chania–Crete, Greece, 2024, 512–521. https://doi.org/10.1109/ICUAS60882.2024.10556898

27. Z. Zhou, H.-Y. Yu, Y.-C. Liu, Fractional-order adaptive fixed-time fault-tolerant control for quadrotor unmanned aerial vehicle, *Commun. Nonlinear Sci. Numer. Simulat.*, **159** (2026), 109884. https://doi.org/10.1016/j.cnsns.2026.109884

AIMS Press